Toxicology in Vitro 50 (2018) 95–108

Contents lists available at ScienceDirect

Toxicology in Vitro

journal homepage: www.elsevier.com/locate/toxinvit

The biological effects of long-term exposure of human bronchial epithelial cells to total particulate matter from a candidate modified-risk tobacco product

Marco van der Toorn*, Alain Sewer, Diego Marescotti, Stephanie Johne, Karin Baumer, David Bornand, Remi Dulize, Celine Merg, Maica Corciulo, Elena Scotti, Claudius Pak, Patrice Leroy, Emmanuel Guedj, Nikolai Ivanov, Florian Martin, Manuel Peitsch, Julia Hoeng, Karsta Luettich

PMI R&D, Philip Morris Products S.A. (Part of Philip Morris International group of companies), Quai Jeanrenaud 5, CH-2000 Neuchâtel, Switzerland

ARTICLE INFO

Keywords:
Lung cancer
Epithelium
Cigarette
Tobacco heating system
Modified-risk tobacco product

ABSTRACT

Cigarette smoking is the leading cause of preventable lung cancer (LC). Reduction of harmful constituents by heating rather than combusting tobacco may have the potential to reduce the risk of LC. We evaluated functional and molecular changes in human bronchial epithelial BEAS-2B cells following a 12-week exposure to total particulate matter (TPM) from the aerosol of a candidate modified-risk tobacco product (cMRTP) in comparison with those following exposure to TPM from the 3R4F reference cigarette. Endpoints linked to lung carcinogenesis were assessed. Four-week 3R4F TPM exposure resulted in crisis and epithelial to mesenchymal transition (EMT) accompanied by decreased barrier function and disrupted cell-to-cell contacts. By week eight, cells regained E-cadherin expression, suggesting that EMT was reversible. Increased levels of inflammatory mediators were noted in cells treated to 3R4F TPM but not in cells treated to the same or a five-fold higher concentration of cMRTP TPM. A 20-fold higher concentration of cMRTP TPM increased oxidative stress and DNA damage and caused reversible EMT. Anchorage-independent growth was observed in cells treated to 3R4F or a high concentration of cMRTP TPM. 3R4F TPM-derived clones were invasive, while cMRTP TPM-derived clones were not. Long-term exposure to TPM from the cMRTP had a lower biological impact on BEAS-2B cells compared with that of exposure to TPM from 3R4F.

1. Introduction

Cigarette smoking is the leading cause of preventable lung cancer (LC) worldwide (Bilello et al., 2002). Quitting smoking is the best way to reduce the risk of LC. In this study, we report in vitro data that indicate that harm from combusted tobacco components may be significantly reduced using tobacco heat-not-burn technology to produce an aerosol or tobacco vapor rather than smoke. Carcinogens in smoke

Abbreviations: A.U., Arbitrary units; BEBM, Bronchial epithelial cell basal medium; BEGM, Bronchial epithelial cell growth medium; BIF, Biological impact factor; CCL5, Chemokine (C-C motif) ligand 5; CDH1, Cadherin-1; CFA, Cell fate network; CIM, Cell invasion migration; cMRTP, Candidate modified-risk tobacco product; COPD, Chronic obstructive pulmonary disease; CPR, Cell proliferation network; CSF-2, Colony-stimulating factor 2; CSF-3, Colony-stimulating factor 3; CTNNB1, Catenin beta 1; CO_2, Carbon dioxide; cRNA, Complementary RNA; CS, Cigarette smoke; CST, Cellular stress network; CXCL-1, Chemokine (C-X-C motif) ligand 1; CXCL-5, Chemokine (C-X-C motif) ligand 1; DDR, DNA damage response; DNA, Deoxyribonucleic acid; DHE, Dihydroethidium; DMSO, Dimethyl sulfoxide; FCS, Fetal calf serum; FDA, Food and Drug Administration; FDR, False discovery rate; fRMA, Frozen robust microarray analysis; GC, Gas chromatography; GSH, Glutathione; EDTA, Ethylene diaminetetraacetic acid; EMT, Epithelial-mesenchymal transition; FDA, Food and Drug Administration; FDR, False discovery rate; FID, Flame ionization detection; H2AX, Histone 2AX; pH2AX, Phosphorylation histone 2AX; γH2AX, Gamma histone 2AX; HCS, High content screening; HECD-1, Mouse monoclonal E Cadherin antibody; HPHC, Harmful and potentially harmful constituents; IL-1A, Interleukin-1 alfa; IL-1B, Interleukin-1 beta; IL-8, Interleukin-8; IPA, Ingenuity pathway analysis; IPN, Inflammatory process network; KEGG, Kyoto Encyclopedia of Genes and Genomes; LC, Lung cancer; mBCL, Monochlorobimane; MET, Mesenchymal-epithelial transition; miRNA, micro Ribonucleic acid; mRNA, messenger Ribonucleic acid; MMP, Matrix metalloproteinase; ND, Not determined; NHBE, Normal human bronchial epithelial; NPA, Network perturbation amplitude; NUSE, Normalized unscaled standard error; RBIF, Relative biological impact factor; RMA, Robust multi-array; RNA, Ribonucleic acid; rpm, Rounds per minute; RTCA-DP, Real-time cell analyzer dual-plate; RTCA-MP, Real-time cell analyzer multi-plate; RLE, Relative log expression; RNA, Ribonucleic acid; ROS, Reactive oxygen species; SDC2, Syndecan-2; SEM, Standard error of the mean; TAGLN, Transgelin; TGF-β, Transforming growth factor beta; THS, Tobacco Heating System; TIMP, Tissue inhibitor of metalloproteinase; TPM, Total particulate matter; TPM1, Tropomyosin alpha-1 chain; TRA, Tissue repair and angiogenesis; VEGF, Vascular endothelial growth factor; VEGFA, Vascular endothelial growth factor A; VIM, Vimentin

* Corresponding author at: Systems Toxicology, Biological Systems Research, Philip Morris International, R&D, Switzerland.
E-mail address: Marco.vanderToorn@pmi.com (M. van der Toorn).

https://doi.org/10.1016/j.tiv.2018.02.019
Received 31 July 2017; Received in revised form 16 February 2018; Accepted 28 February 2018
Available online 07 March 2018

produced during the combustion and pyrolysis of tobacco elicit genotoxic and non-genotoxic mechanisms underlying lung carcinogenesis (Bersaas et al., 2016; Bilello et al., 2002; Hecht et al., 2016). Heating tobacco at a temperature below that required to initiate combustion generates an aerosol with significantly lower levels of harmful and potentially harmful constituents (HPHC) while maintaining the nicotine yield (Smith et al., 2016).

LC is a complex disease characterized by genetic and epigenetic aberrations that are reflected in morphological and phenotypic changes of the bronchial and alveolar epithelium over time (Smith et al., 1996). To confirm the potential for disease risk reduction of any new candidate modified-risk tobacco product (cMRTP), epidemiological studies are needed. However, owing to the long latency period between cigarette smoke (CS) exposure and disease development, evidence in support of this risk reduction may not be available for decades. Therefore, an approach that leverages short-term data for long-term risk assessment is needed. Although the direct translation of a complex disease, such as LC, to an in vitro model is quite challenging, many aspects of the carcinogenic process, including genetic damage and cellular transformation, can be modeled adequately in cell culture systems. In this study, we evaluated the functional and molecular changes during long-term exposure of human bronchial epithelial cells to total particulate matter (TPM) from a new cMRTP, the Tobacco Heating System (THS) 2.2, in comparison with those following exposure to TPM from the 3R4F reference cigarette. THS 2.2 is a battery-operated heating system into which a tobacco stick is inserted and heated in a controlled manner. The heating system operates at a maximum temperature of 350 °C, which generates a tobacco aerosol that is primarily composed of water, glycerol, and nicotine (Schaller et al., 2016; Smith et al., 2016). In contrast, during the combustion of conventional cigarettes, the temperature of the tobacco increases up to 900 °C, resulting in > 6000 combustion and pyrolysis tobacco components (Baker, 1974; Rodgman and Perfetti, 2013). The U.S. Food and Drug Administration (FDA) has established a list of HPHCs in tobacco products and tobacco smoke that are linked to the five most serious health effects of tobacco use. FDA classified 79 of these HPHCs as carcinogenic to humans (FDA, 2012). TPM, which represents the particulate phase of mainstream CS, comprises approximately 80% of the total weight of CS (Barsanti et al., 2007) and is made up of many organic and inorganic components as well as solid particles. Many of the carcinogens are present in TPM (Rodgman and Perfetti, 2013). Therefore, in this study, TPM was used as a test item to investigate the effects of the mixture of cancer-causing chemicals present in CS on a cancer model system in vitro and to compare these effects with those of the TPM from THS 2.2 aerosol.

To assess functional and molecular changes over time, a human-immortalized bronchial epithelial cell line, BEAS-2B, was continuously exposed to TPM from 3R4F CS and three different concentrations of TPM from THS 2.2 aerosol for 12 weeks. BEAS-2B cells are considered normal, non-clonogenic cells and do not form tumors in nude mice. In contrast to 2D cultures of primary human bronchial epithelial cells, which are not suitable for this type of long-term experiment because of their limited life span, BEAS-2B cells are immortal. Together with wild-type p53 and a functional DNA repair system (Reddel et al., 1995), these features make BEAS-2B cells a useful model for the assessment of MRTPs. This study demonstrates that repeated exposure of BEAS-2B cells to TPM from 3R4F CS induces ongoing alterations in gene expression as well as phenotypic changes, such as epithelial-mesenchymal transition (EMT) and anchorage independence. Furthermore, our findings suggest that fewer carcinogens in the TPM from THS 2.2 aerosol, which results from heating rather than combusting tobacco, may be responsible for its limited effects on BEAS-2B cells when compared with those elicited by 3R4F TPM exposure.

2. Methods

2.1. Chemicals

Rotenone, ethacrynic acid, chlorambucil, transforming growth factor-beta (TGF-β), dimethyl sulfoxide (DMSO), β-mercaptoethanol, n-butyl acetate, trimethylamine, and isoquinoline were obtained from Sigma-Aldrich (Deisenhofen, Germany). Collagen A was obtained from Biochrom AG (Berlin, Germany). Hoechst dye was purchased from Thermo Fisher Scientific Inc. (Reinach, Switzerland). Anti-pH2AX (05-636) antibody was purchased from Merck Millipore (Schaffhausen, Switzerland). Anti-HECD-1 (ab1416) and anti-vimentin (ab45939) antibodies were purchased from Abcam (Cambridge, UK). Dylight 550 and 650 secondary antibodies, dihydroethidium (DHE), monochlorobimane (mBCL), Geltrex® Ready-To-Use matrix, and RPMI 1640 medium were purchased from Life Technologies (Zug, Switzerland). Fetal calf serum (FCS), penicillin, and streptomycin were obtained from GE Healthcare (Zurich, Switzerland). Bronchial Epithelial Basal Medium™ (BEBM™), and SingleQuots™ kits were obtained from Lonza (Basel, Switzerland). RNeasy lysis buffer was obtained from Qiagen (Hilden, Germany). Human metalloproteinase (MMP) (HMMP2MAG-55K), tissue inhibitor of metalloproteinase (TIMP) (HTMP2MAG-54), and cytokine/chemokine (HCYTOMAG-60K) magnetic bead panels were obtained from Merck Millipore (Schaffhausen, Switzerland).

2.2. Cell culture

The human bronchial epithelial cell line BEAS-2B was obtained from the American Type Culture Collection (LGC Standards, Wesel, Germany). A mycoplasma test was carried out by Public Health England (Porton Down, UK). Cell line authentication has been carried out by the American Type Culture Collection using the short tandem repeat profiling method (ATCC, Manassas, USA). BEAS-2B cells were cultured in Bronchial Epithelial Cell Growth Medium (BEGM™), consisting of BEBM™ supplemented with a SingleQuots™ kit, following the vendor's recommendations. Cells were grown in 75 cm^2 collagen I-coated culture flasks (VWR, Dietikon, Switzerland) at 37 °C in an atmosphere of 5% CO_2 until reaching 75%–80% confluence. A CASY® counter was used to count cells and assess cell viability according to the manufacturer's instructions (Roche Diagnostics, Mannheim, Germany).

2.3. Generation of 3R4F and THS 2.2 TPM

3R4F reference cigarettes were purchased from the University of Kentucky (Lexington, KY, USA; http://www.ca.uky.edu/refcig/). THS 2.2 sticks and tobacco stick holders were provided by Philip Morris Products S.A. (Neuchâtel, Switzerland). THS 2.2 operates by inserting a specially designed tobacco stick into a holder that heats the tobacco plug to generate an aerosol containing water, glycerin, nicotine, and tobacco flavors with reduced concentrations of harmful constituents compared with CS (Schaller et al., 2016; Smith et al., 2016). The tobacco stick holder includes a battery, electronics for control, a heating element, and stick extractor. Prior to use in the study, 3R4F and THS 2.2 sticks were conditioned according to ISO Standard 3402 for at least 48 h at a temperature of 22 ± 1 °C and a relative humidity of 60 ± 3% before being used for smoke or aerosol generation. Smoke from 3R4F cigarettes was generated on a 20-port Borgwaldt smoking machine (Hamburg, Germany), and aerosol from THS 2.2 was generated on a 30-port SM2000/P1 smoking machine (Philip Morris International, Neuchâtel, Switzerland) according to the Health Canada Intense protocol (55 mL puff volume; 2 s puff duration; 2 min^{-1} puff frequency; 100% blocking of 3R4F filter ventilation holes) (Health Canada, 1999). TPM (containing organic and inorganic compounds) from the mainstream smoke of 3R4F reference cigarettes or aerosol from THS 2.2 sticks was trapped on glass fiber filters, from which it was then extracted with an appropriate volume of DMSO to give a final concentration of 100 mg

TPM/mL. This procedure was repeated three times to prepare three independent 3R4F and THS 2.2 TPM batches.

2.4. TPM nicotine analysis

To monitor batch consistency of the TPM, the amount of nicotine was quantified as follows. After TPM extraction, an aliquot of 100 µL TPM was transferred to a vial containing 900 µL n-butyl acetate, 0.1% trimethylamine, and isoquinoline as internal standard. Nicotine analyses using a gas chromatograph (GC) with flame ionization detection (FID) were performed on an Agilent 7890A GC (Agilent Technologies; Basel, Switzerland) equipped with a standard flame ionization detector. The GC was equipped with a J&W capillary column, DB-5 15 m × 0.25 mm ID fused silica film 0.25 µm (Agilent Technologies). The GC inlet was maintained at 220 °C with a constant flow (1.4 mL/min) of ultrapure helium (Carbagas, Gümligen, Switzerland) as the carrier gas. Ultra zero air (Carbagas) and ultrahigh-purity hydrogen (Carbagas) were used for the flame ionization detector. An injection split ratio of 1:50 was used for these analyses. The GC oven was isotherm at 140 °C for 2.5 min. Total GC run time was 2.5 min. All GC-FID analyses were performed once per batch.

2.5. Chronic exposure of BEAS-2B

Three different cryopreserved stock vials of BEAS-2B cells were cultured independently in cell culture flasks over 12 weeks. At designated time points (Monday and Friday of each week), media were removed, and cells were rinsed and passaged. On Mondays and Fridays, cells (0.5×10^6 cells and 1.0×10^6, respectively) were seeded in 75 cm^2 collagen I-coated culture flasks (VWR) and grown at 37 °C in an atmosphere of 5% CO_2. Six hours after seeding, BEAS-2B cells were exposed to a low concentration of TPM from 3R4F cigarette smoke (7.5 µg/mL) or low, medium, and high concentrations of TPM from THS 2.2 aerosol (7.5, 37.5 or 150 µg/mL). Each of the three biological replicates was exposed to a different batch of TPM. The actual concentration of nicotine in 3R4F TPM (2.5 µM) applied to the cell culture was 2.5 times higher than the concentration of nicotine found in the lungs of active smokers (approximately 1.0 µM). Similarly, the equivalent nicotine concentrations of the medium and high THS 2.2 TPM treatments were five and 20 times higher (medium dose, 6.0 µM; high dose, 24 µM), while the low concentration was comparable (1.2 µM) to that seen in smokers' lungs (Catassi et al., 2008; Olale et al., 1997). Cells containing medium with 0.15% (*v*/v) DMSO were included as a vehicle control. At regular intervals, cells and supernatants were collected for mRNA and protein analysis. For a more detailed exposure and sample collection scheme, see Fig. 1 in the supplementary data.

2.6. High-content screening

After one, two, four, eight, and 12 weeks of TPM exposure, BEAS-2B cells from three independently cultured stock vials were seeded in quadruplicate for each condition in black collagen I-coated, clear-bottom 96-well tissue culture plates (BD, Allschwil, Switzerland) at a density of 1.2×10^4 cells/well for high-content screening-based analysis of oxidative stress, DNA damage, and EMT marker expression. Twenty-four hours after seeding, cells were incubated in the presence of a positive control and vehicle control (DMSO) before the high-content assays were conducted. Oxidative stress was assessed using DHE fluorescence with rotenone at a final concentration of 100 µM as a positive control. Glutathione was measured using mBCL, and 500 µM ethacrynic acid served as the assay's positive control. Chlorambucil (100 µM) was used to induce DNA damage, which was detected by a specific antibody targeting pH2AX. EMT was induced by treatment with 5 µg/mL TGF-β and monitored via antibody-based analysis of E-cadherin and vimentin expression. Following staining of the nucleus with Hoechst dye, fluorescence data were acquired with a Cellomics® ArrayScan™ VTI HCS Reader (Thermo Fisher Scientific Inc., Waltham, MA, USA) and vHCS view software (Thermo Fisher Scientific Inc.). Twenty fields were imaged per well using a 10× wide-field objective.

2.7. Epithelial cell adhesion assay

The effects of chronic TPM exposure on epithelial cell adhesion were evaluated using *E*-plates and an xCELLigence® Real-Time Cell Analyzer Multi-Plate (RTCA-MP) instrument (ACEA Biosciences, San Diego, CA, USA). The well bottoms were coated with collagen A for 1 h before seeding 1.2 × 104 BEAS-2B cells/well from three independently cultured stock vials in quadruplicate for each condition on the inserts of the coated *E*-plates containing BEGM™ medium. Changes in the cell index (impedance) were recorded and measured in real time during cell adhesion. A high and stable cell index was reached when the BEAS-2B cells covered the entire bottom of the *E*-plate.

2.8. Protein analysis

The levels of several cytokines and chemokines, including interleukin (IL)-1, IL-6, IL-8, tumor necrosis factor alpha (TNFα), vascular endothelial growth factor (VEGF), tissue inhibitor of metalloproteinase (TIMP), and matrix metalloproteinase (MMP), were determined in duplicate in supernatants from three independently cultured BEAS-2B stock vials using the MILLIPLEX® MAP Human Cytokine/Chemokine and Human TIMP and MMP magnetic bead panels (Merck Millipore) with Luminex technology according to the manufacturer's instructions.

2.9. Cell transformation assay and recovery of clones

Three cryopreserved stock vials of BEAS-2B cells were cultured independently over 12 weeks and constantly exposed to TPM from 3R4F CS and THS 2.2 aerosol as described above. Thereafter, cells were trypsinized, seeded in duplicate for each condition, and processed according to the manufacturer's instructions for the CytoSelect™ 96-well Cell Transformation Assay (Cell Biolabs, San Diego, CA, USA). Fluorescence was monitored with an excitation wavelength of 485 nm through a 520-nm band pass filter in a 96-well fluorimeter (FLUOstar Omega microplate reader, BMG Labtech, Ortenberg, Germany). Anchorage-independent clones were collected from the agar according to the manufacturer's instructions (Cell Biolabs) and stored in liquid N_2.

2.10. Epithelial cell invasion assay

The rate of cell invasion was monitored in real time using cell invasion migration (CIM) plates and an xCELLigence® RTCA-DP instrument (ACEA Biosciences). The electrode surface of the CIM plate was coated with collagen A for 1 h. The membrane of the CIM plate was coated with Geltrex® Ready-To-Use as extracellular matrix component. Four cryopreserved stock vials of 3R4F and THS 2.2 TPM-derived BEAS-2B colonies were grown overnight in BEBM™. The next day, 4.0×10^4 cells were seeded in each well of the upper chamber in BEBM™. The lower chambers were filled with BEBM™ containing 10% FCS or no serum as a negative control. The CIM plate was left in an incubator for 15 min before recording cell migration. Thereafter, changes in the cell index (impedance), reflecting cell invasion, were recorded in real time and analyzed using RTCA software 2.0 (ACEA Biosciences). The slope of the invasion cell index curves during a selected time period was calculated by fitting the points to a straight line.

2.11. RNA extraction and microarray hybridization

From all three biological replicates of each experimental condition, 0.5×10^6 BEAS-2B cells were collected after 1, 2, 4, 8, and 12 weeks of exposure for transcriptomic analysis. A full randomization was applied across all collected samples prior to sample processing to minimize

batch effects. Cells were lysed in 240 µL RLT lysis buffer containing 1% β-mercaptoethanol, followed by RNA extraction using a QIAGEN miRNeasy Mini Kit (QIAGEN). The quantity of purified RNA was determined using the NanoDrop™ ND8000 spectrophotometer (Thermo Fisher Scientific), while the quality of the RNA was analyzed using an Agilent 2100 Bioanalyzer (Agilent). Only RNA samples with an RNA integrity number (RIN) ≥ 6 were processed further. The target preparation workflow was performed using the Biomek FXP Target Prep Express liquid handling system (Beckman Coulter, Brea, CA, USA). Total RNA (100 ng) was reverse-transcribed to cDNA using the Gene Chip® HT 3′ IVT PLUS kit (Affymetrix, Santa Clara, CA, USA). The cDNA was then labeled, amplified to complementary RNA (cRNA), and fragmented. Successful fragmentation was confirmed using the Agilent 2100 Bioanalyzer, and hybridization cocktails were prepared for each sample according to the manufacturer's instructions. The final cocktails were hybridized to GeneChip® Human Genome U133 Plus 2.0 Arrays (Affymetrix) at 45 °C for 16 h while rotating at 60 rpm. Arrays were then washed and stained on a GeneChip® Fluidics Station FS450 DX (Affymetrix) using the protocol FS450_0001, and scanned using a GeneChip® Scanner 3000 7G (Affymetrix) to generate the CEL files containing the gene expression raw data. The FlashTag™ Biotin HSR kit (Affymetrix) was used to label miRNA. Two hundred nanograms of total RNA, containing low molecular weight RNA, were subjected to a tailing reaction, followed by ligation of the biotinylated signal molecule to the target RNA sample. The GeneChip® miRNA 4.0 arrays (Affymetrix) were incubated for 16–18 h at 48 °C while rotating at 60 rpm. Arrays were washed and stained on a GeneChip® Fluidics Station FS450 DX (Affymetrix) with protocol FS450_0002 and scanned using a GeneChip® Scanner 3000 7G (Affymetrix) to generate the CEL files containing the miRNA raw data.

2.12. Gene expression analysis

The raw data CEL files were preprocessed through a standard computational pipeline that uses Bioconductor packages implemented in the R statistical software environment (Huber et al., 2015; Team, R.C., 2014) as follows: The raw data quality was first checked by examining several quality metrics implemented in the affyPLM and affy packages including log-intensities plots, normalized unscaled standard error (NUSE) plots, relative log expression (RLE) plots, polyA controls boxplots, RNA degradation plots, spike-in control boxplots, and pseudo- and raw microarray images (Brettschneider et al., 2008; Gautier et al., 2004). The 75 delivered CEL files all passed the quality controls, which used a set of predefined acceptance thresholds. The raw data were then background-corrected, and normalized, and summarized using frozen robust microarray analysis (fRMA) (McCall et al., 2010). Probe set summarization was applied to generate microarray expression values from all arrays using the custom CDF environment HGU133-Plus2_Hs_ENTREZG v16.0 (Dai et al., 2005). A moderated statistical method implemented in the limma R package was used to identify significantly regulated genes (Smyth, 2005). Linear models containing the biological replicate number as a covariate were defined to estimate the effects of interest, and raw *p*-values were calculated for each probe set. The Benjamini-Hochberg false discovery rate (FDR) method was then applied to adjust the raw *p*-values for multiple testing effects (Benjamini and Hochberg, 1995). Adjusted *p*-values below 0.05 were considered statistically significant. The data have been deposited in the Array Express database (https://www.ebi.ac.uk/arrayexpress/) under accession number E-MTAB-5697.

2.13. Network analysis

Gene expression profiles induced by exposure to TPM from 3R4F CS or THS 2.2 aerosol were analyzed in the context of a collection of hierarchically structured network models describing the molecular mechanisms underlying essential biological processes in healthy lung tissues (Boue et al., 2015). The network perturbation amplitude (NPA) scoring method leverages high-throughput measurements and a priori literature-derived knowledge in the form of network models to characterize activity changes for a broad collection of biological processes at high resolution.

The NPA itself aims to reduce high-dimensional transcriptomics data by combining the gene expression fold-changes into fewer differential network backbone node values (between a few dozen and two hundred). By definition of the two-layer structure of the network models, no measurements corresponding to nodes in the upper "functional" layer are available. The differential network backbone node values will therefore be determined by a fitting procedure that infers values that best satisfy the directional and signed relationships contained in the backbone model upper functional layer, while being constrained by the experimental data (the log2-fold-changes for the genes constituting the lower "transcript" layer). NPA summarizes into a single number how well and how strongly the inferred values match with the network, and the resulting score serves as a basis for further interpretation. However, since a significant NPA score (with respect to the biological variation) alone does not indicate whether the gene fold-changes specifically reflect the network structure itself, so-called companion statistics, O and K, are employed. Assessing (1) the adequacy of the downstream genes (transcript layer) assignment to the nodes of the backbone model by reshuffling the gene labels in the transcript layer (O), and (2) the importance relevance of the cause-and-effect relationships encoded in the backbone of the network in extracting the NPA scores (K), respectively, enables significant O and K *p*-values (typically below 0.05) to indicate that the network is specifically perturbed. The key contributors to the perturbation, referred to as "leading nodes, are by definition the nodes that make up 80% of the NPA score, and this score accounts for both the differential backbone values themselves and the centrality of the nodes in the functional layer. To assess the amplitude of perturbation induced by the different culture conditions defined in this study, the NPA was computed for all contrasts using a pre-selection of sub-network models. NPA scores were then aggregated into a unique value termed the biological impact factor (BIF), summarizing the overall perturbation of the biological system (Thomson et al., 2013).

2.14. MicroRNA expression analysis

The miRNA microarray raw data from the CEL files were preprocessed through a standard pipeline. CEL files were read by the read.celfiles function of the oligo Bioconductor package developed for the R statistical software environment (Carvalho and Irizarry, 2010; Huber et al., 2015; Team, R.C., 2014). The array quality was controlled using the arrayQualityMetrics package (Kauffmann et al., 2009), and four distinct metrics were examined: The Euclidean distances between arrays in the raw data matrix, the Euclidean distances between arrays in the normalized data matrix, the NUSE values, and the probe intensity distributions. Arrays that were found to be outliers in at least two of the metrics were discarded, and the quality was re-examined on the remaining arrays until all were accepted. This approach led to discarding five arrays out of 75 in one iteration. These five arrays were regenerated together with their matching control samples sharing the same biological replicate numbers, in order to reduce the impact of repetition on the pairwise "exposure vs. control" comparisons (see below). These 10 additional CEL files passed the above quality controls. The normalized probe-level data were then obtained by applying a robust multi-array (RMA) normalization and by summarizing at probe set-level using the median polish method (Bolstad et al., 2003; Irizarry et al., 2003).

The Affymetrix GeneChip® miRNA 4.0 arrays simultaneously probe the expression of 30,424 mature miRNAs belonging to 203 species, among which 2578 are human. Using the annotation provided by Affymetrix and the latest miRBase nomenclature (release 21, June 2014) (Griffiths-Jones et al., 2006), all probe sets pertaining to non-

human species were filtered out. Following Affymetrix' instructions, only the miRNA probe sets that have significantly higher intensity values than their matched background probes (based on GC content and sequence length) should be considered "detected". A significant threshold of 0.001 was selected for determining the detection calls based on Wilcoxon tests. If a miRNA probe set was detected in 75% of the samples of at least one sample group, it was kept for downstream analysis; if not, it was discarded. This preprocessing approach yielded 455 miRNA probe sets in the final normalized expression matrix after exclusion of the control probe sets. In order to focus on miRNAs that are more likely to be functionally relevant in the exposure responses, it was meaningful to consider the "high confidence" miRNAs defined by miRBase (Kozomara and Griffiths-Jones, 2014), which constituted a subset of 150 mature miRNA probe sets.

For each pairwise "exposure vs. control" comparison, a submatrix of the global normalized expression matrix was derived by retaining only the samples belonging to the exposure or the control groups, as well as the miRNA probe sets that were detected in 75% of the samples of at least one of the two groups. Similarly to the case of gene expression, a moderated statistics method implemented in the limma package was used to identify significantly regulated miRNA probe sets based on linear models containing the biological replicate number as a covariate (Smyth, 2005). Raw *p*-values were generated for each retained miRNA, and the Benjamini-Hochberg multiple test adjustment method was then applied (Benjamini and Hochberg, 1995). MiRNA probe sets with adjusted *p*-values below 0.05 were considered statistically significant. The data have been deposited in the Array Express database under accession number E-MTAB-5698.

2.15. Statistics

Data are expressed as mean ± standard error of the mean (SEM) of values derived from three biological replicates unless otherwise indicated. Comparisons between different experimental groups were performed with one-way ANOVA using GraphPad Prism version 6.03 (GraphPad Software, Inc., La Jolla, CA, USA). When the overall F test of the ANOVA analysis was significant ($p < 0.05$), Dunnett's multiple comparison test was applied to determine the sources of differences, which were considered to be statistically significant when $p < 0.05$. Statistical analysis was performed using SAS software version 9.2 (SAS, Wallisellen, Switzerland) on data from Luminex-based measurements. Values were transformed using natural log transformation and comparisons were made using a paired *t*-test.

3. Results

3.1. Nicotine analysis of TPM from 3R4F and THS 2.2

Both THS 2.2 and CS have particulate phases that can be trapped on glass fiber pads and is termed TPM. The nature of the TPM from each product, however, is very different. Quantification of overall TPM and nicotine from each of the products is shown in Fig. 1. No differences were observed between the amount of TPM captured from 3R4F CS and THS 2.2 aerosol (Fig. 1A). Nicotine concentrations were significantly lower in TPM from THS 2.2 aerosol than in TPM from 3R4F CS (Fig. 1B).

3.2. Chronic exposure of BEAS-2B cells to TPM from 3R4F CS and THS 2.2 aerosol at a 20-fold higher concentration induces functional changes over time

We first tested the effect of TPM from 3R4F CS and THS 2.2 aerosol on primary normal human bronchial epithelial (NHBE) cells from multiple donors. The results indicate that NHBE cells undergo a limited, predetermined number of cell divisions before entering senescence (data not shown). We therefore decided to use BEAS-2B cells, a SV40-immortalized human bronchial epithelial cell line that was previously shown to be a suitable model for cancer risk assessment in vitro (Clancy et al., 2012; Costa et al., 2010; Jing et al., 2012). BEAS-2B cells were continuously exposed to 7.5 μg/mL 3R4F TPM or to 7.5, 37.5 and 150 μg/mL of THS 2.2 TPM for 12 weeks. Several endpoints, including proliferation, oxidative stress, DNA damage, and EMT, were assessed at regular intervals by cell counting (CASY® counter), high-content analysis, and xCELLigence® real-time impedance measurements (Fig. 2). After the first week of exposure to 3R4F TPM, a significant increase in DHE fluorescence was observed compared with the vehicle (DMSO) control ($p < 0.001$), indicating a rise in intracellular reactive oxygen species (ROS) levels. Thereafter, DHE fluorescence decreased. Chronic exposure of BEAS-2B cells to different doses of THS 2.2 TPM decreased the levels of DHE fluorescence compared with the vehicle control. Surprisingly, a 20-fold higher concentration of THS 2.2 TPM (150 μg/mL) showed the strongest decrease in DHE fluorescence at all time points. Next, the levels of intracellular glutathione (GSH), an important radical scavenger which plays a key role in the cellular redox status of cells and tissues, were assessed. Intracellular GSH was measured using the non-fluorescent substrate mBCL, which forms fluorescent adducts with GSH in a reaction catalyzed by glutathione-S-transferase. The first 4 weeks of exposure of BEAS-2B cells to TPM from 3R4F CS or a 20-fold higher concentration of THS 2.2 TPM significantly increased levels of mBCL fluorescent adducts ($p < 0.01$), indicating an increase in intracellular GSH. Thereafter, mBCL fluorescence decreased to the same level as that seen in the vehicle control, with the exception of week 8 values where fluorescence was somewhat lower. This may have been related to high variability in individual measurements, leading to a high standard deviation of mBCL fluorescence. Chronic exposure of BEAS-2B cells to an equal or a 5-fold higher concentration of THS 2.2 TPM did not affect GSH levels compared with the vehicle control.

Oxidative stress and a cellular redox imbalance cause serious damage to cells, leading to the development of oxidative DNA damage (Ganapathy et al., 2015). Therefore, pH2AX was evaluated as an indicator of oxidative stress-mediated double-strand DNA breaks. Chronic exposure of BEAS-2B cells to TPM from 3R4F CS or 5- and 20-fold higher concentrations of THS 2.2 TPM significantly increased pH2AX during the first 2 weeks of treatment, but this effect subsided thereafter, indicating adaptation to the chronic stress of exposure. Cell cycle checkpoints are regulatory pathways that respond to DNA damage – collectively termed the DNA damage response (DDR) – by arresting the cell cycle to provide time for repair and by inducing transcription of genes that facilitate repair (Elledge, 1996). Results show that exposure to TPM from 3R4F CS or THS 2.2 aerosol at 20-fold higher concentrations arrested the cell cycle by significantly decreasing cell numbers on week 4 ($p < 0.0001$). Thereafter, cell numbers recovered, suggesting that cells may have become accustomed to the presence of TPM. Furthermore, no significant differences in cell numbers were observed when cells were chronically exposed to an equal or 5-fold higher concentration of THS 2.2 TPM.

Next, we assessed EMT, a process by which epithelial cells lose their polarity and cell-cell adhesion (Kalluri and Weinberg, 2009; Xiao and He, 2010). Cell-cell adhesion was detected by staining adherent junctions of epithelial cells for E-cadherin, whereas cells that undergo the EMT process could be detected by the expression of the mesenchymal protein vimentin. After 4 weeks of treatment, 3R4F TPM and a 20-fold higher concentration of THS 2.2 TPM increased the levels of vimentin, with concomitant loss of epithelial E-cadherin, indicating that EMT had occurred. This observation was in line with a decrease in the BEAS-2B cell index, a value that mirrors cell-matrix adhesion. After 8 to 12 weeks, cells regained E-cadherin expression and cell-matrix adhesion, suggesting that EMT was reversible. No significant effects were observed when cells were chronically exposed to an equal or 5-fold higher concentration of THS 2.2 TPM.

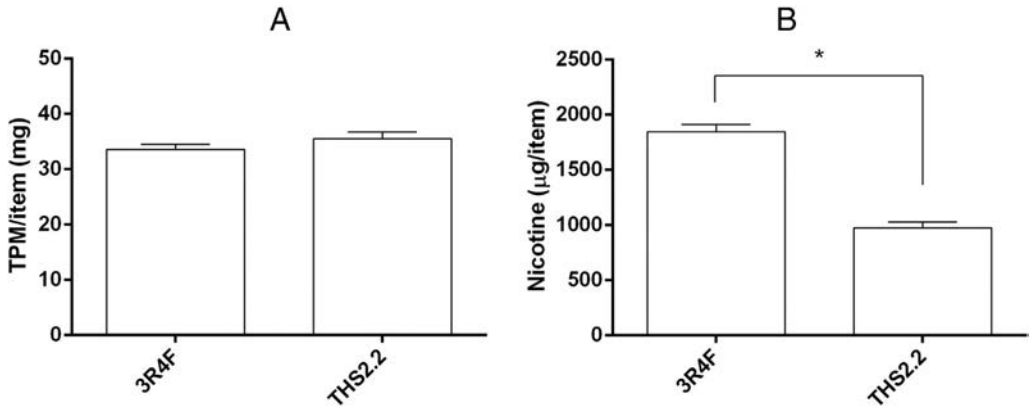

Fig. 1. Nicotine analysis in TPM from 3R4F cigarette smoke and THS 2.2 aerosol. A) Concentration of TPM in mg per test item. B) Nicotine analysis of TPM in µg per test item. Data are presented as mean ± SEM of values from three independently generated batches. $^{*}p < 0.05$ vs. 3R4F by paired *t*-test. TPM: Total particulate matter; 3R4F: Reference cigarette; THS 2.2: Tobacco Heating System 2.2.

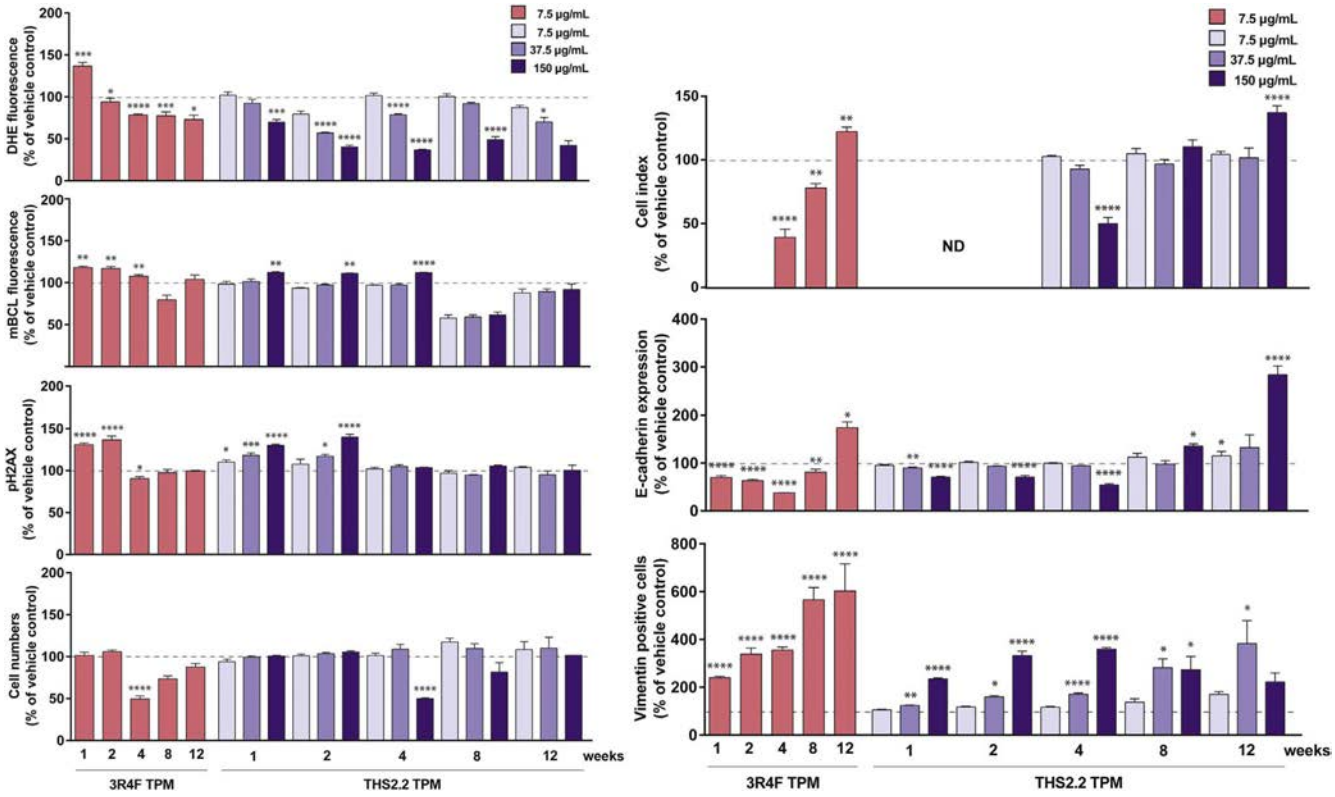

Fig. 2. Functional changes over time during chronic exposure of BEAS-2B to TPM from 3R4F (red bars) and three different concentrations of THS 2.2 (purple bars). High-content analysis of oxidative stress (DHE), glutathione (mBCL), double-strand DNA breaks (pH2AX), epithelial mesenchymal transition (E-cadherin, vimentin) in BEAS-2B cells over time, expressed as % of DMSO (vehicle) control. Proliferation using a CASY counter (cell numbers), and real-time impedance-based analysis (cell index) to monitor cell-matrix adhesion in BEAS-2B cells over time are expressed as % of the vehicle (DMSO) control. Data are expressed as mean ± SEM of values derived from three biological replicates. $^{*}p < 0.05$ vs. vehicle; $^{**}p < 0.01$ vs. vehicle; $^{***}p < 0.001$ vs. vehicle; $^{****}p < 0.0001$ vs. vehicle by Dunnett's multiple comparison test. DHE: Dihydroethidium; mBCL: Monochlorobimane; pH2AX: Phosphorylation of histone 2AX; EMT: Epithelial-mesenchymal transition; ND: not determined; TPM: Total particulate matter; 3R4F: Reference cigarette; THS 2.2: Tobacco Heating System 2.2. (For interpretation of the references to color in this figure legend, the reader is referred to the web version of this article.)

3.3. Chronic exposure of BEAS-2B cells to TPM from 3R4F CS and THS 2.2 aerosol at a 20-fold higher concentration induces inflammatory processes over time

In addition to oxidative stress and DNA damage, chronic exposure of airway epithelial cells to CS or CS components has been shown to cause inflammation (Hoffmann et al., 2013; Li et al., 2016; Mijosek et al., 2016) and alter migratory and invasive properties (Son et al., 2012). Therefore, a select number of mediators released into the cell culture supernatant over time were evaluated using Luminex technology. All analytes were above the limits of quantification. Fold changes of mediator levels relative to the vehicle controls are depicted as a heatmap in Fig. 3. Exposure of BEAS-2B cells to 3R4F TPM caused a rapid increase in IL1A, IL-8 (CXCL8), CXCL1, CSF-2, CSF-3, VEGFA, MMP-1, MMP-9, and TIMP-1 levels, while CCL5, CXCL10, and TIMP-2 levels decreased. With few exceptions, these elevated levels were maintained over the duration of treatment, with additional increases in IL-6 levels from week 2 onward. Similarly, CXCL10 and TIMP-2 levels remained significantly lower in 3R4F TPM-exposed cells compared with levels in vehicle controls, while CCL5 concentrations slowly recovered to reach a > 6-fold increase over vehicle controls by week 12. BEAS-2B cells exposed to an equal concentration of THS 2.2 TPM, however, only exhibited an increase in MMP-1 levels on weeks 1, 2, and 12, and TIMP-2 levels decreased on weeks 1 and 4. Exposure to a 5-fold higher THS 2.2 TPM concentration caused an increase in CXCL-1, CSF3, MMP-1, and VEGF levels, and a decrease in CCL2, CXCL10, and TIMP-2 levels,

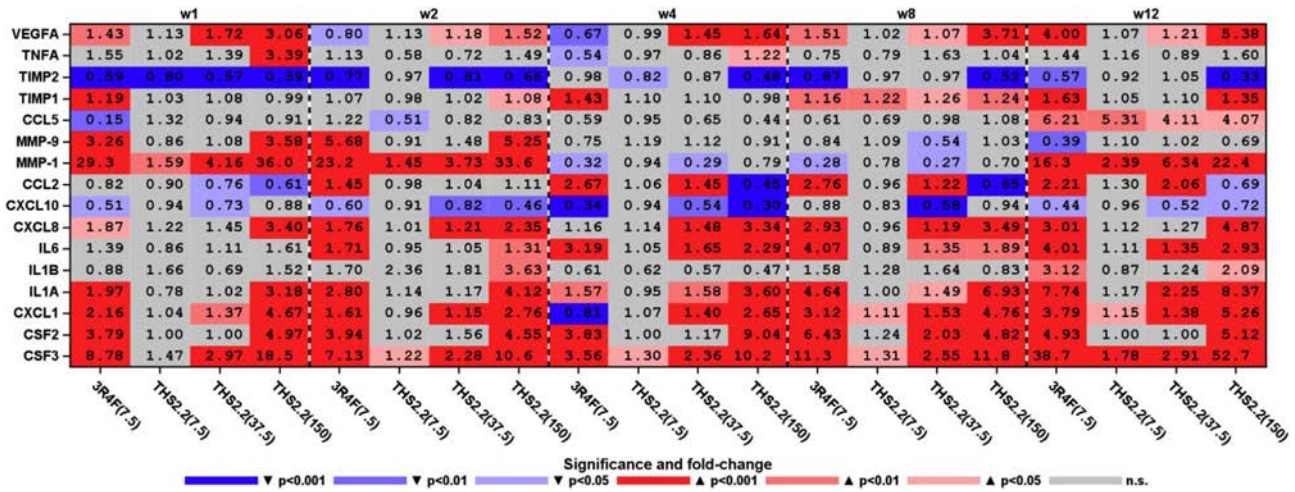

Fig. 3. Quantification of inflammatory mediators secreted by TPM-treated BEAS-2B cells into the cell culture medium over time. Cell-free supernatants derived from three biological replicates were analyzed using a multiplexed bead array. Data are presented as a heatmap indicating fold changes compared with DMSO control. Significant differences are highlighted in bold and color-coded for significant increase (red shades) and decrease (blue shades) as indicated using a paired *t*-test ($p < 0.05$). Values in grey represent fold changes that were not statistically significant ($p > 0.05$). 3R4F: Reference cigarette; THS 2.2: Tobacco Heating System 2.2. (For interpretation of the references to color in this figure legend, the reader is referred to the web version of this article.)

albeit not to the same extent as that seen in the supernatants from 3R4F TPM-treated cells. Finally, exposure of BEAS-2B cells to the highest THS 2.2 TPM concentration elicited a similar response in soluble mediator release as exposure to 3R4F TPM.

3.4. 3R4F TPM-transformed BEAS-2B cells display characteristics of EMT

To determine whether the chronic exposure to TPM caused cellular transformation, we seeded BEAS-2B cells exposed to TPM from 3R4F CS and THS 2.2 aerosol for 12 weeks in soft agar. Colonies that arose from individual cells were quantified using a fluorescent assay. Anchorage-independent growth was only observed in BEAS-2B cells exposed to 3R4F TPM, although not statistically significant, and a 20-fold higher concentration of THS 2.2 TPM (Fig. 4A). Neither vehicle nor exposure to an equal or a 5-fold higher THS 2.2 TPM concentration led to colony formation of the BEAS-2B cells in soft agar. Clones from treated BEAS-2B cells (3R4F TPM and THS 2.2 TPM at a 20-fold higher concentration) were retrieved from the agar and subsequently grown as monolayer cultures in the absence of TPM. Thereafter, the invasion capacity of the transformed BEAS-2B cells was tested. 3R4F TPM-derived clones were invasive, while THS 2.2 TPM-derived clones were not (Fig. 4B). To ascertain the occurrence of EMT, expression of vimentin and E-cadherin was assessed in the 3R4F and THS 2.2 TPM-derived clones. Fig. 4C clearly shows EMT of the 3R4F TPM-derived clones compared with cells from the vehicle control. While the THS 2.2 TPM-derived clones displayed a unique morphology compared with cells from the vehicle control, the occurrence of a complete EMT was inconclusive.

3.5. Chronic exposure of BEAS-2B cells to TPM from 3R4F CS and a 20-fold higher concentration of THS 2.2 TPM induces gene and miRNA expression changes over time

Relative gene and miRNA expression changes of BEAS-2B cells were determined after 1, 2, 4, 8, and 12 weeks of exposure to TPM from 3R4F CS (7.5 µg/mL) and THS 2.2 aerosol (7.5, 37.5, and 150 µg/mL). Quality control of the microarray data was performed to ensure that they were of high quality and not affected by experimental replicate, experimental condition, or batch effects (data not shown). Exposure to an equal or a 5-fold higher concentration of THS 2.2 TPM resulted in no or only a few changes in differentially expressed mRNA levels in BEAS-2B cells over time (adjusted *p*-value < 0.05; Table 1).

Extracellular matrix protein tenascin C (TNC), involved in the survival and metastasis of lung cancer cells (Parekh et al., 2005), was among the few genes affected early on by TPM treatment. *TNC* mRNA expression levels in BEAS-2B cells were initially > 5-fold higher than vehicle control levels following exposure to 3R4F TPM (weeks 1 and 2), and remained elevated (approximately 2-fold change over controls) over the remainder of the exposure period. While no changes were observed in *TNC* expression levels following exposure to an equal concentration of THS 2.2 TPM, exposure to a 5-fold higher concentration caused a ca. 2-fold increase in *TNC* gene expression on weeks 2 and 4, without noticeable changes compared with controls at later time points. Other genes whose expression levels were affected throughout the exposure period included a number of genes encoding chemokines and cytokines (e.g., *IL6*, *CCL2*, *CXCL1*, *CXCL3*, *CXCL8*, *IL1B*) and structural proteins (e.g., *VIM*, *TAGLN*, *CTNNB1*, *TPM1*, *SDC2*, *CDH1*). Generally, 3R4F TPM exposure caused greater dysregulation of gene expression than exposure to THS 2.2 TPM at a 5-fold higher concentration. Exposure of BEAS-2B to TPM from 3R4F CS and a 20-fold higher THS 2.2 TPM concentration caused a time-dependent increase in the number of significantly differentially expressed genes, with a maximum increase observed at 4 and 8 weeks of exposure (3R4F TPM vs. vehicle: 1658 genes up- and 2101 down-regulated; 150 µg/mL THS 2.2 TPM vs. vehicle: 1662 genes up- and 2310 down-regulated; adjusted *p*-values < 0.05).

Although there was a considerable overlap in the genes affected by both treatments and the direction in which the expression changed, gene expression fold changes tended to be greater with 3R4F TPM treatment. Following exposure of BEAS-2B cells to TPM from 3R4F CS and a 20-fold higher THS 2.2 TPM concentration, gene-set enrichment analysis indicated statistically significant enrichments of genes positively associated with inflammatory responses, complement and coagulation cascades, steroid synthesis, and cell structure, as well as in terms of genes negatively associated with developmental processes, stemness, and amino acid metabolism. The underlying KEGG gene sets were taken from the graphite package (Sales et al., 2012), and the enrichment calculations were performed using the piano package (Varemo et al., 2013).

Similar to the changes in gene expression levels, significant changes in miRNA expression levels were absent or limited in BEAS-2B cells exposed to THS 2.2 TPM at an equal or a 5-fold higher concentration than 3R4F TPM. Long-term exposure to 3R4F TPM, however, caused dysregulation of substantially more miRNAs over time, with miR-503-5p, miR-424-3p, miR-182-5p and miRNA-200 family members (among

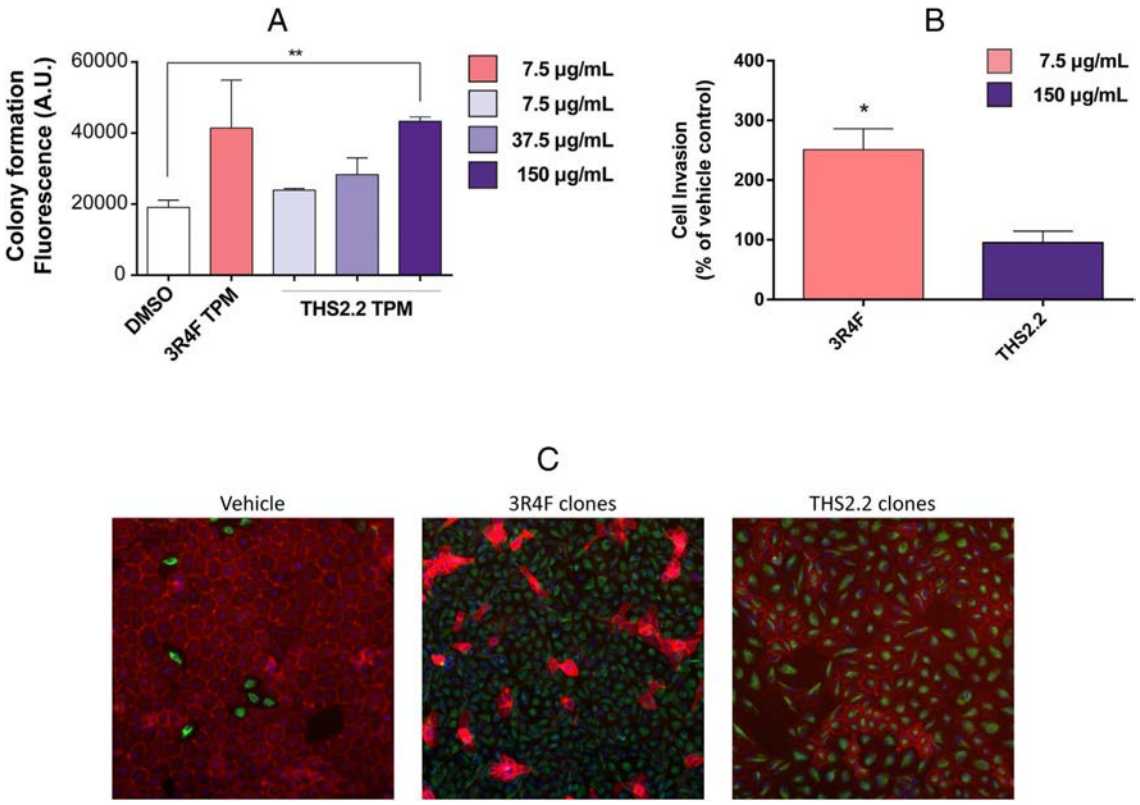

Fig. 4. A–C. Anchorage-independent growth, invasiveness, and EMT of transformed BEAS-2B cells. A) Cellular transformation was assessed after exposing BEAS-2B cells for 12 weeks to TPM from 3R4F and three different concentrations of THS 2.2. Transformed cells were collected from the agar and tested for B) invasiveness and C) epithelial mesenchymal transition (expression of vimentin and E-cadherin). Cell transformation was determined by measuring the formation of cell colonies using a fluorescent dye to eliminate manual cell counting. The capacity of transformed BEAS-2B cells to invade through a Geltrex coating was measured in real time using xCELLigence technology. Representative high-content images of BEAS-2B cells exposed for 12 weeks to vehicle and agar-isolated clones from 3R4F or high-concentration THS 2.2-exposed BEAS-2B cells stained for Hoechst (blue), vimentin (green), and E-cadherin (red) selected from random fields are shown. Cell transformation data are expressed as mean ± SEM of values derived from three biological replicates. Cell invasion data of isolated BEAS-2B colonies are expressed as mean ± SEM of values derived from four biological replicates. $^{*}p < 0.05$ vs. vehicle and $^{**}p < 0.01$ vs. vehicle control by paired *t*-test. 3R4F: Reference cigarette; THS 2.2: Tobacco Heating System 2.2; A.U.: Arbitrary units. (For interpretation of the references to color in this figure legend, the reader is referred to the web version of this article.)

others) significantly down-regulated, and miRNA-140-3p, miR-138-1-3p, miRNA-29a-3p, miRNA-19b-3p, miRNA-222-3p, miRNA-29b-1-5p, miRNA-155-5p and miRNA-138-5p significantly up-regulated on week 3. In most cases, expression of these affected miRNAs remained dysregulated in treated cells, before returning to levels seen in vehicle controls. Only miRNA-222-3p, miRNA-29b-1-5p, miRNA-155-5p and miR-138-5p expression consistently increased throughout the exposure period. This was also true for BEAS-2B cells exposed to a 20-fold higher concentration of THS 2.2 TPM. However, in those cells, expression of a number of miRNAs, including miR-1910-5p, miR-29a-3p, miRNA-222-3p, miRNA-100-5p, miRNA-29b-1-5p, miRNA-31-5p, miRNA-92a-1-5p and miR-155-5p, was already significantly up-regulated after week 1 of treatment, and in most cases levels returned to those in vehicle controls thereafter. Other miRNAs, such as miR-130b-3p, miR-17-5p, miR-106a-5p, miRNA-18a-5p, miRNA-25-5p, miRNA-92a-3p, miRNA-20a-5p and miRNA-3613-3p, exhibited increased expression levels only much later, after 12 weeks of treatment. Although miRNA-155-5p expression levels were significantly elevated also in BEAS-2B cells exposed to 150 µg/mL THS 2.2 TPM over 12-week period, expression of miR-27b-3p and miR-149-5p decreased earlier and more markedly compared with expression following 3R4F TPM treatment. Of note, miRNA-106a-5p, miRNA-210-3p, miRNA-25-5p, miRNA-1910-5p, miRNA-92a-3p, miRNA-20a-5p were significantly up- and miRNA-30c-5p, miRNA-15b-5p, miRNA-15a-5p, miRNA-7d-5p, miRNA-7f-5p were significantly down-regulated following exposure to THS 2.2 TPM, independent of concentration, but not following 3R4F TPM treatment.

Table 1
Gene and miRNA expression changes over time.

The number of significantly differentially expressed genes (left) and miRNA (right) in three biological replicates of BEAS-2B cells exposed to 3R4F TPM or three different doses of THS 2.2 TPM compared with the vehicle control over time are shown (adjusted *p*-value < 0.05).

	Differentially expressed genes					Differentially expressed miRNAs				
	w1	w2	w4	w8	w12	w1	w2	w4	w8	w12
3R4F (7.5 µg/mL)	1003	1791	3745	3760	2664	0	3	25	113	69
THS 2.2 (7.5 µg/mL)	0	0	0	0	0	0	0	20	0	0
THS 2.2 (37.5 µg/mL)	0	4	34	26	6	0	0	1	0	0
THS 2.2 (150 µg/mL)	1643	1356	3972	1519	3357	21	33	15	53	41

TPM: total particulate matter; 3R4F: reference cigarette; THS 2.2: Tobacco Heating System 2.2; w: week.

3.6. Chronic exposure of BEAS-2B cells to TPM from 3R4F and a 20-fold higher concentration of THS 2.2 TPM induces significant network perturbations over time

Network analysis was used to identify molecular mechanisms that may be linked to cellular transformation in BEAS-2B cells after long-term exposure to TPM from 3R4F CS or THS 2.2 aerosol. The network analysis uses the reverse approach, in which genes that have been described in the literature as being regulated by an upstream biological entity (such as a transcription factor) are grouped together. The assumption is then made that the upstream entity is perturbed if the corresponding gene group displays a "collective" differential expression. Since this method is used without threshold for the statistical significance of individual gene differential expressions, it can be considered more sensitive than other, commonly used gene expression analysis tools (Kogel et al., 2015; Martin et al., 2014; Martin et al., 2012). We consider a network perturbation to be significant when the three associate statistics are significant, as explained in the "Methods" section ("Network Analysis" subsection). The various network perturbations are summarized by the higher-level BIF metric that provides a mechanistic overview of the biological impact of the applied treatment. The highest biological impact was seen in BEAS-2B cells exposed to 3R4F TPM for 8 weeks (relative BIF = 100% −this treatment will be the reference "REF" for all the relative BIF values). A lower magnitude of network perturbation was observed in BEAS-2B cells exposed to 3R4F for 1, 2, 4, and 12 weeks, although with similar underlying sub-network perturbations, as indicated by the high δ values (Fig. 5). The biological impact of BEAS-2B cells exposed to a 20-fold higher concentration of TPM from THS 2.2 aerosol for 4 weeks was similar in magnitude and underlying sub-network perturbation relative to the 3R4F TPM treatment. However, the relative BIF declined from week 8 onward, and the extent of network perturbation for BEAS-2B cells exposed to the highest THS 2.2 TPM concentration was notably smaller on week 12 than that seen in BEAS-2B cells exposed to 3R4F TPM. Cells exposed to an equal or a 5-fold higher concentration of THS 2.2 TPM exhibited very low-magnitude biological impact, and the underlying sub-network perturbation was different relative to the 3R4F TPM reference (Fig. 5). DMSO, used as a vehicle control, did not cause any network perturbations relative to medium (data not shown).

The biological mechanisms covered by the networks included cell fate (CFA), cell proliferation (CPR), cellular stress (CST), lung inflammation (IPN), and tissue repair and angiogenesis (TRA). Each network was constructed in a modular way, in which each module or sub-network describes a specific biological aspect of the entire network. Fig. 6 shows a heatmap of all the subnetworks that were significantly perturbed by chronic exposure to TPM. Based on the contributions across the comparisons, the two most prominent networks involved globally were the CFA and IPN networks. These perturbations were predominantly driven by perturbations of the Apoptosis, Senescence, Epithelial Innate Immune Activation, and Tissue Damage sub-networks across the contrasts. Exposure of BEAS-2B cells to 3R4F TPM resulted in a higher level of network perturbation and a higher number of perturbed networks compared with exposure to an equal or a 5-fold higher concentration of THS 2.2 TPM, with a maximum perturbation on week 8, as indicated by the relative BIF. A comparable network perturbation and number of perturbed sub-networks (except for the Xenobiotic Metabolism Response sub-network) were found when comparing the exposure to highest THS 2.2 TPM concentration with the exposure to vehicle control. In addition, the maximum perturbation following exposure to a 20-fold higher concentration of THS 2.2 TPM was detected at an earlier stage (4 weeks) compared with perturbation following 3R4F TPM exposure (Fig. 6).

3.7. Chronic exposure of BEAS-2B cells to TPM from 3R4F and a 20-fold higher concentration of THS 2.2 TPM induces significant miRNA expression changes over time

Fig. 7 shows a heatmap of the fold changes of individual miRNAs in BEAS-2B cells in response to chronic exposure to TPM. Fifty-three miRNAs showed a statistically significant (adjusted p-value < 0.05) difference in abundance in at least one exposure group compared with the DMSO group. Exposure of BEAS-2B cells to 3R4F TPM resulted in 40 statistically significant differentially expressed miRNAs at one or more time points. Exposure to an equal or a 5-fold higher concentration of THS 2.2 TPM resulted in ≤3 significantly differentially expressed miRNAs. BEAS-2B cells exposed to a 20-fold higher concentration of THS 2.2 TPM yielded 37 significantly differentially expressed miRNAs at one or more time points. MicroRNA-155 was the most strongly up-regulated miRNA at all-time points, which was also seen following 3R4F TPM treatment. Furthermore, a 12-week exposure to 20-fold higher concentration of THS 2.2 TPM resulted in more significantly differentially expressed miRNAs compared with 3R4F TPM treatment. Interestingly, a number of miRNAs related to EMT, including miRNA-503, miRNA-424 and miRNA-200b-3p (Abba et al., 2016), were significantly down-regulated in BEAS-2B cells exposed to 3R4F TPM or a 20-fold higher concentration of THS 2.2 TPM in week 4 and 8 relative to the DMSO controls.

4. Discussion

Carcinogens in CS are responsible for airway epithelial cell transformation. To compare the biological effects of long-term exposure of BEAS-2B cells to TPM from the aerosol of a new cMRTP, THS 2.2, in comparison with TPM from the smoke of 3R4F reference cigarettes, functional and molecular endpoints were assessed over a 12-week period. In this study, repeated exposure of BEAS-2B cells to 3R4F TPM increased the production of ROS and caused DNA damage within the first 2 weeks, but these effects subsided by week 4, indicating adaptation to the chronic stress. Four-week exposure of BEAS-2B cells to 3R4F TPM, however, resulted in cellular crisis and EMT. This EMT was accompanied by a decrease in barrier function and disruption of cell-to-cell contacts. By week 8, cells regained proliferative capacity and E-

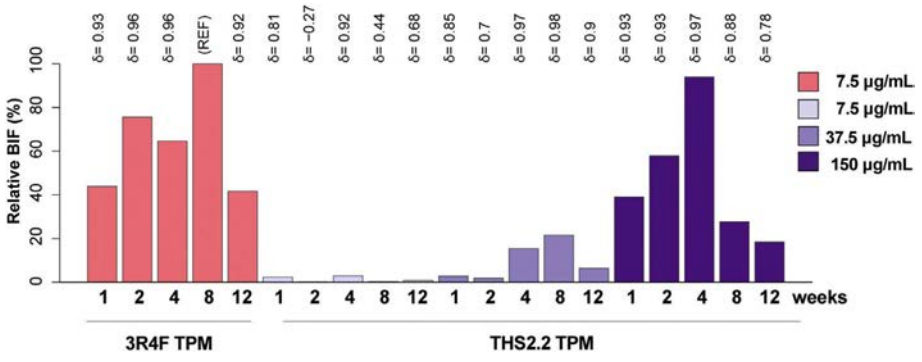

Fig. 5. Relative biological impact factor (RBIF) analysis of BEAS-2B cells exposed to 3R4F total particular matter (TPM) or three different doses of THS 2.2 TPM compared with vehicle over time. RBIF calculations were based on gene expression data sets from three biological replicates and each condition per time point. The percentages give the RBIF, which is derived from the cumulated network perturbations caused by the exposure relative to the reference, showing the highest perturbation (3R4F 8 weeks vs DMSO, RBIF = 100%). For each exposure comparison, the δ value (−1 to 1) indicates how similar the underlying network perturbations are with respect to the reference (REF).

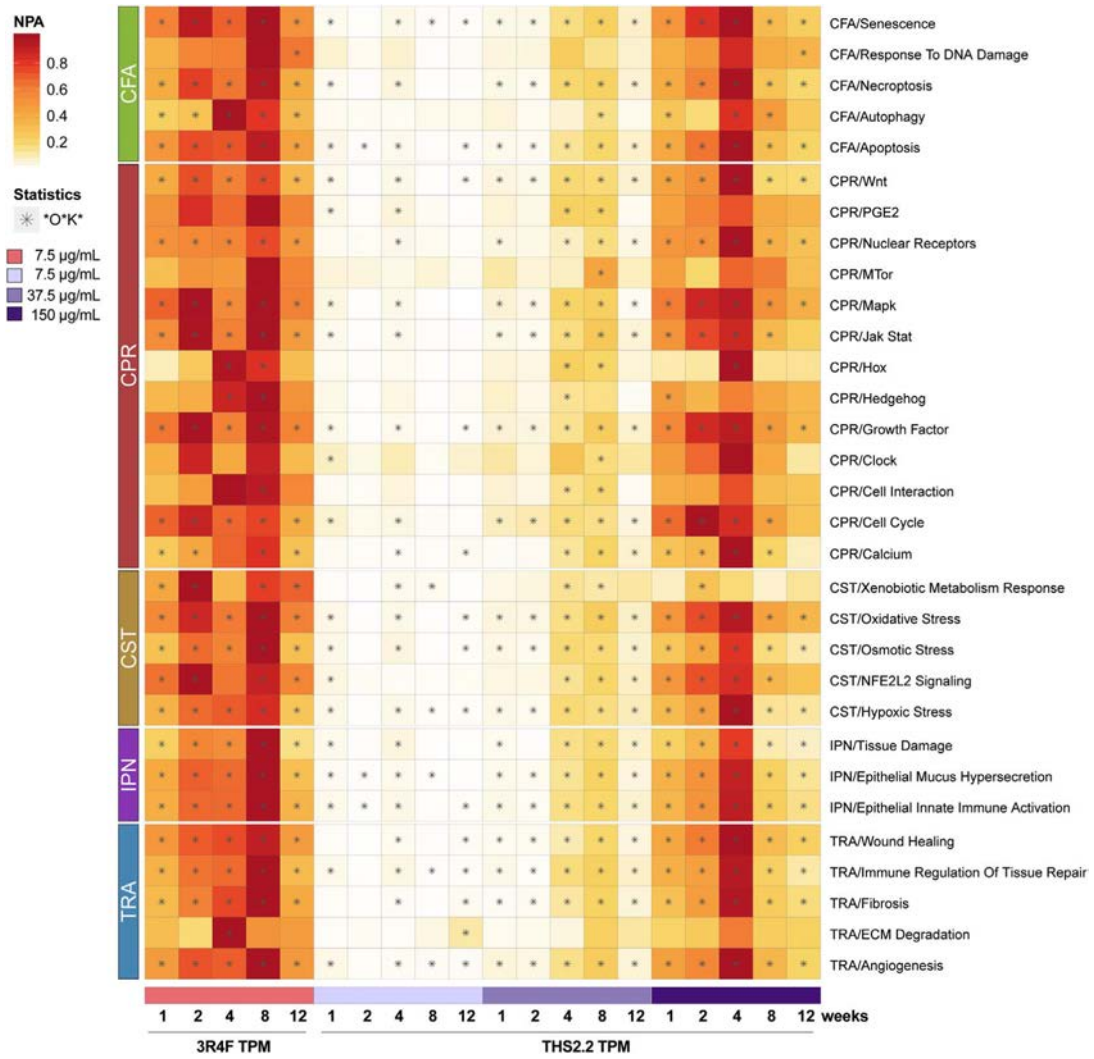

Fig. 6. Biological impact of exposures of BEAS-2B cells to 3R4F TPM or three different doses of THS 2.2 TPM over time compared with vehicle control on computational network models. The biological impact was calculated using the Cell Fate (CFA), Cell Proliferation (CPR), Cell Stress (CST), Lung Inflammation (IPN), and Tissue Regeneration and Angiogenesis (TRA) networks. NPA calculations were based on gene expression data sets from three independent biological replicates and each condition per time point. The heatmap summarizes significant perturbed biological networks and subnetworks at 1, 2, 4, 8, and 12 weeks in response to the different treatments. The biological networks are listed on the right and their respective subnetworks are listed on the left. A network is considered perturbed if, in addition to the significance of the network perturbation amplitude (NPA) score with respect to the experimental variation, the two companion statistics (O and K) derived to inform on the specificity of the NPA score with respect to the biology described in the network are significant. Symbol legend: *: O and K statistic *p*-values below 0.05 and significant with respect to the experimental variation.

cadherin expression, suggesting that EMT was reversible. Time-dependent increases in levels of angiogenic proteins, growth factors, and inflammatory cytokines were noted in cells exposed to 3R4F TPM. We also found that repeated exposure of BEAS-2B cells to TPM from 3R4F CS significantly altered gene expression. However, prolonged exposure of BEAS-2B cells to the same or a 5-fold higher concentration of TPM from THS 2.2 aerosol relative to 3R4F TPM did not markedly change cellular, functional, and molecular endpoints (Fig. 8). In addition, anchorage-independent growth was only observed in BEAS-2B cells exposed to 3R4F TPM and a 20-fold higher concentration of THS 2.2 TPM. We found that the 3R4F TPM-derived clones were mesenchymal and invasive, while the THS 2.2 TPM-derived clones were not.

CS is known to contain many carcinogens associated with ROS generation (Valavanidis et al., 2009). An imbalance between ROS generation and safe detoxification generates oxidative stress, a recognized oncogenic risk factor. Increased oxidative stress, mimicked by the chronic exposure of BEAS-2B cells to TPM, is known to activate a variety of pro-inflammatory transcription factors, including NF-κB, AP-1, p53, HIF-1α, PPAR-γ, β-catenin/Wnt, and Nrf2. Activation of these transcription factors can lead to the expression of growth factors, inflammatory cytokines, and chemokines, as well as cell cycle regulatory molecules (Reuter et al., 2010). Inflammatory cells are present in tumors, and tumors arise at sites of chronic inflammation. For example, patients with chronic obstructive pulmonary disease (COPD), which is a lung disease characterized by chronic inflammation, are at increased risk for the development of lung cancer (Durham and Adcock, 2015; Oh and Sin, 2012). Our gene expression data are mirrored by the Luminex analysis and suggest that sustained exposure to TPM from 3R4F CS or a 20-fold higher concentration of THS 2.2 aerosol induces a self-perpetuating cycle of inflammation in BEAS-2B cells. In line with this, the Epithelial Innate Immune Activation sub-network was strongly perturbed across these contrasts. ROS are the chemical effectors that link inflammation and genetic alteration to carcinogenesis by directly causing oxidation, nitration, and halogenation of DNA, RNA, and lipids (Federico et al., 2007). In this study, we measured double-strand DNA breaks, which are considered the most lethal form of DNA damage, severely compromising genomic stability (Mah et al., 2010). BEAS-2B cells exposed to TPM from 3R4F CS and a 20-fold higher concentration of THS 2.2 TPM showed increased levels of phosphorylated histone variant H2AX, known as γH2AX, indicating increased double-strand

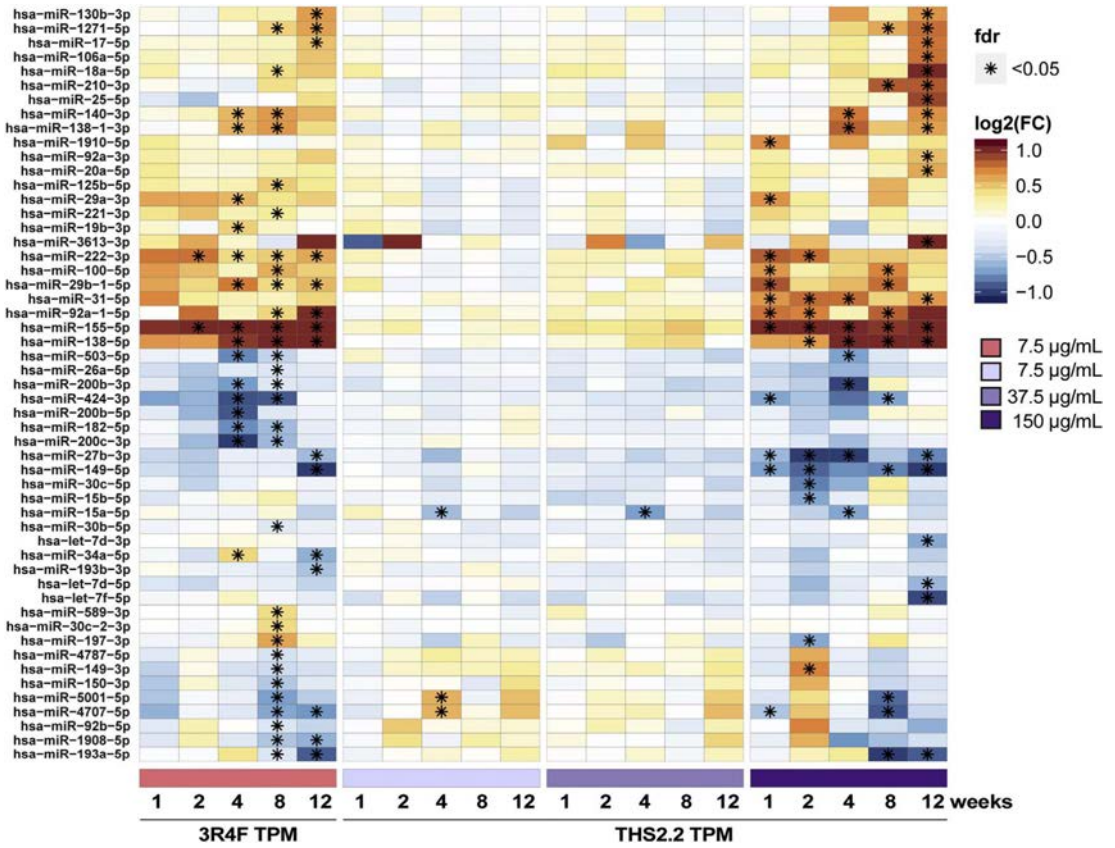

Fig. 7. Differential expression of individual miRNAs from three biological replicates (all pairwise comparisons). Heatmap displays the fold changes in BEAS-2B cells in response to the different treatments compared with the vehicle control and the associated statistical significance for miRNAs at 1, 2, 4, 8, and 12 weeks. Only miRNAs with an adjusted *p*-value below 0.05 in at least one of the 20 pairwise comparisons are shown. The miRNAs were ordered by standard clustering based on Euclidean distance.

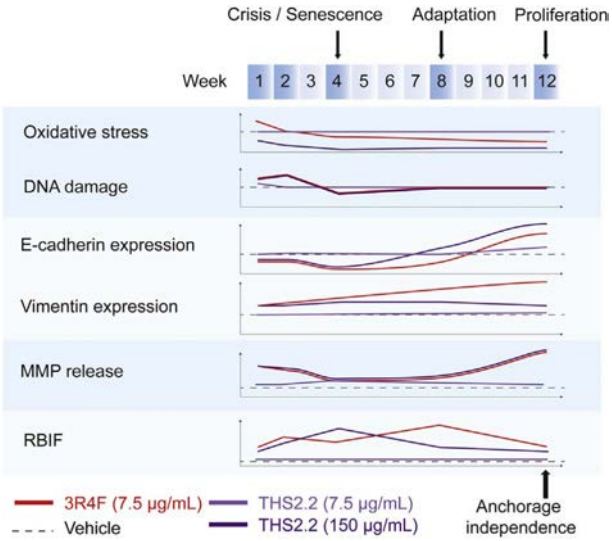

Fig. 8. Functional and molecular changes associated with cellular transformation during long-term exposure of human bronchial epithelial cells to TPM from THS 2.2 in comparison with TPM from 3R4F reference cigarette.

DNA damage. Although computational network analysis did not show an early perturbation of the DNA Damage sub-network, a significant perturbation of this sub-network was observed when BEAS-2B cells were exposed long-term to TPM from 3R4F CS or a 20-fold higher concentration of THS 2.2 TPM. Immediate and efficient error correction following DNA damage is important to restore and preserve chromatin architecture (Mah et al., 2010). A series of DNA pathways comprising the DNA damage response are responsible for the recognition, signaling, and repair of DNA damage in cells. Cells exhibiting too much DNA damage or cells that can no longer effectively repair DNA damage enter a state of senescence or initiate apoptosis (Grigoryeva et al., 2015). Our data show that BEAS-2B cells exposed to TPM from 3R4F CS or a 20-fold higher concentration of THS 2.2 TPM for 4 weeks undergo cellular crisis, during which there is a slowing of cellular growth. Computational network analysis indicated a strong perturbation of the Apoptosis and Senescence sub-networks, with a maximum perturbation amplitude during the cellular crisis. These results suggest that when effective repair fails, the integrity of the genome would be protected by senescence or elimination of damaged cells from the cycling population through programmed cell death.

Lung epithelial cells are characterized by cell-cell interactions, formation of intercellular and basolateral junctions, polarized distribution of cellular components, and lack of mobility (Dasari et al., 2006). During the long-term exposure of BEAS-2B cells to TPM from 3R4F CS and THS 2.2 aerosol, we observed a change in epithelial morphology and phenotype. One of the first critical morphological and phenotypic alterations of epithelial cells that may drive carcinogenesis is the EMT process, by which epithelial cells lose their polarity and intercellular and basolateral junctions, and become highly mobile (Kalluri and Weinberg, 2009). In the present study, decreased E-cadherin expression and concomitantly increased levels of vimentin after 4 weeks of exposure to 3R4F TPM or a 20-fold higher concentration of THS 2.2 TPM were accompanied by morphological changes typical of EMT. This notion was further supported by the observed dysregulation of a number of miRNAs and genes encoding structural proteins known to be linked to EMT (Momi et al., 2014; Zhao et al., 2015). Interestingly, following 8 to 12 weeks of TPM treatment, a reversal of this process, termed mesenchymal-epithelial transition (MET), which involves the

conversion of the mesenchymal phenotype back to the epithelial phenotype, appeared to have occurred.

Most of the signals inducing EMT exert their effects through the modulation of transcription factors that repress epithelial genes and activate genes associated with the mesenchymal phenotype (Moreno-Bueno et al., 2008). Transcription factors which drive EMT are members of the Snail, basic helix-loop-helix (Twist) families, and two double zinc finger and homeodomain (ZEB) factors. These EMT transcription factors can be regulated by post-transcriptional mechanisms. In this study, we found increased expression of miRNA-155 and miRNA-138, two positive modulators of EMT (Ding, 2014; Zhang et al., 2016), in the cells exposed to 3R4F TPM or a 20-fold higher concentration of THS 2.2 TPM. MicroRNAs can also suppress EMT by up-regulating E-cadherin and inhibiting EMT transcription factors (Guo et al., 2014; Moreno-Bueno et al., 2008). In line with this finding, decreased expression of miRNA-503, miRNA-424, and miRNA-200b-3p, all known to suppress EMT (Abba et al., 2016), were found when BEAS-2B cells were exposed to 3R4F TPM or a 20-fold higher concentration of THS 2.2 TPM for 4 and 8 weeks. Silencing EMT transcription factors leads to partial reversion of the epithelial phenotype (Guo et al., 2014; Moreno-Bueno et al., 2008). Our results show that expression of all detected EMT repressor miRNAs reversed in week 12. This may explain the observed partial conversion of mesenchymal cells back to the epithelial phenotype.

The accumulation of step-wise functional and molecular changes occurring in this in vitro model system appears to be insufficient to reprogram the majority of the BEAS-2B cells to undergo cellular transformation in response to chronic exposure to TPM. BEAS-2B cells exhibit wild-type p53 and a functional DNA repair system (Reddel et al., 1995), and therefore have limited adaptive capacity. Thus, they are unable to bypass the negative effects of TPM treatment, although a few cells attained an independent survival advantage. One of the escape mechanisms to undergo cellular transformation is the accumulation of modifications in the genetic program to bypass DNA repair, cell cycle checkpoints, and density-dependent inhibition of cell proliferation (Boyle and Levin, 2008). Irreparable DNA damage, especially in the critical region of oncogenes and tumor suppressor genes, overcomes the apoptotic and senescent safeguards against inappropriate cell division. We detected significant alterations in the expression of several mRNAs and miRNAs associated with cellular survival over time. These alterations are also quite frequently detected in the tumor tissue of lung cancer patients who are current or former smokers (Gibbons et al., 2014; Zeilinger et al., 2013). In the present study we demonstrate that a small number of BEAS-2B cells were able to escape from the majority of normal BEAS-2B cells after 12 weeks of TPM exposure by showing anchorage-independent growth.

The 3R4F TPM-derived clones were mesenchymal and invasive, while the clones derived from cells exposed to a 20-fold higher concentration of THS 2.2 TPM were not. A major question that remains to be investigated is the effects of TPM exposure on the genome (and epigenome) and how these effects (e.g. mutations) correlate with cell transformation. A study performed by Sun et al., to select BEAS-2B cells for anchorage-independent growth following chronic chromate exposure, indicated a low incidence of spontaneous transformation to the neoplastic phenotype (Sun et al., 2011). More importantly, chromate-transformed BEAS-2B cells were able to form tumors in immune-deficient mice while anchorage-independent clones that arose spontaneously did not, a finding that indicates that chromate-dependent transformation discriminates the induction of an altered cell type from a preexisting cell type. Another issue that remains to be investigated is whether transformed cells with a mesenchymal phenotype and enhanced invasive capability can be more metastatic compared with non-mesenchymal and non-invasive tumorigenic cells. A recent study by Morata-Tarifa et al. confirmed that cultured breast and colon cancer cells with a mesenchymal phenotype and low adherent properties have a higher metastatic and tumor-initiating capacity in immune-deficient mice than cells with a low mesenchymal phenotype and high adherent properties (Morata-Tarifa et al., 2016). A more detailed in vivo xenograft study would be required to further elucidate the tumor-initiating and metastatic potential of the 3R4F and THS 2.2 TPM-derived clones.

We are aware of the fact that repeated exposures to TPM instead of whole smoke or aerosol, the use of a cell line instead of primary cells as well as the use of 2D monolayer culture instead of 3D cell culture systems are limitations of the current study. We attempted to perform the experiments of this study on primary bronchial epithelial cells grown in monolayers. Unfortunately, the limited replication potential (life span) of these cells precluded any long-term exposure set-up. We previously also conducted several studies testing the acute effects of whole CS exposure on bronchial 3D organotypic cultures at the air-liquid interface (Iskandar et al., 2017; Talikka et al., 2014). At this time, we are not equipped to extend such experiments beyond short-term exposure set-ups. This is mainly due to 1) the amount of tissues needed for one 12-week experiment accommodating the series of endpoints we have employed here, and 2) the challenge of keeping the 3D tissues sterile when exposing on a daily basis for weeks or even months. Aside from these technical or logistic issues, it is questionable whether 3D cultures, which are mimics of terminally differentiated tissues and have very limited proliferation potential, would be amenable to long-term exposure experiments of this nature. While it is possible that, in such a case, the differentiated cells of the 3D organotypic cultures will be ablated following exposure over time, leaving basal cells that could be stimulated to proliferate and perhaps even undergo a selection process similar to the one we observed with BEAS-2B cells, we would expect their ultimate fate to be similar to that of primary bronchial epithelial cells grown in 2D monolayers. Without doubt, more studies are needed to address such experimental issues.

5. Conclusions

This study demonstrated that repeated exposure of BEAS-2B cells to TPM from the aerosol of THS 2.2, in comparison with TPM from the smoke of the 3R4F reference cigarette, induced ongoing alterations in gene expression, as well as phenotypic changes such as EMT and anchorage independence, both indicators of cellular transformation. Long-term exposure to TPM from the THS 2.2 heat-not-burn tobacco product had a lower dose-dependent biological impact on human bronchial epithelial cells in comparison with TPM from a combusted tobacco product.

Supplementary data to this article can be found online at https://doi.org/10.1016/j.tiv.2018.02.019.

Transparency document

The http://dx.doi.org/10.1016/j.tiv.2018.02.019 associated with this article can be found, in online version.

Availability of data and material

The data have been deposited in the Array Express database under accession number E-MTAB-5697 for mRNA and E-MTAB-5698 for miRNA.

Competing interests

All authors are employees of Philip Morris International.

Funding

Philip Morris International is the sole source of funding and sponsor of this project.

Authors' contributions

MT, EG, FM, JH, and KL conceived and designed the experiments. MT, DM, SJ, KB, DB, RD, CM, MC, and CP performed the experiments. NI supervised and revised gene expression data. MT, AS, ES, PL, and FM analyzed the data. MT, KL, MP, AS, JH, and NI participated in drafting and revising the manuscript.

Acknowledgements

We thank Dr. S. Ansari for his assistance with biobanking and Dr. S. Boue for the preparation of Fig. 8.

References

Abba, M.L., Patil, N., Leupold, J.H., Allgayer, H., 2016. MicroRNA regulation of epithelial to mesenchymal transition. J. Clin. Med. 5.

Baker, R.R., 1974. Temperature distribution inside a burning cigarette. Nature 247, 405–406.

Barsanti, K.C., Luo, W., Isabelle, L.M., Pankow, J.F., Peyton, D.H., 2007. Tobacco smoke particulate matter chemistry by NMR. Magn. Reson. Chem. 45, 167–170.

Benjamini, Y., Hochberg, Y., 1995. Controlling the false discovery rate: a practical and powerful approach to multiple testing. J. R. Stat. Soc. Ser. B Methodol. 289–300.

Bersaas, A., Arnoldussen, Y.J., Sjoberg, M., Haugen, A., Mollerup, S., 2016. Epithelial-mesenchymal transition and FOXA genes during tobacco smoke carcinogen induced transformation of human bronchial epithelial cells. Toxicol. in Vitro 35, 55–65.

Bilello, K.S., Murin, S., Matthay, R.A., 2002. Epidemiology, etiology, and prevention of lung cancer. Clin. Chest Med. 23, 1–25.

Bolstad, B.M., Irizarry, R.A., Åstrand, M., Speed, T.P., 2003. A comparison of normalization methods for high density oligonucleotide array data based on variance and bias. Bioinformatics 19, 185–193.

Boue, S., Talikka, M., Westra, J.W., Hayes, W., Di Fabio, A., Park, J., Schlage, W.K., Sewer, A., Fields, B., Ansari, S., Martin, F., Veljkovic, E., Kenney, R., Peitsch, M.C., Hoeng, J., 2015. Causal biological network database: a comprehensive platform of causal biological network models focused on the pulmonary and vascular systems. Database (Oxford) 2015, bav030.

Boyle, P., Levin, B., 2008. World Cancer Report 2008. IARC Press, International Agency for Research on Cancer Lyon.

Brettschneider, J., Collin, F., Bolstad, B.M., Speed, T.P., 2008. Quality assessment for short oligonucleotide microarray data. Technometrics 50, 241–264.

Carvalho, B.S., Irizarry, R.A., 2010. A framework for oligonucleotide microarray preprocessing. Bioinformatics 26, 2363–2367.

Catassi, A., Servent, D., Paleari, L., Cesario, A., Russo, P., 2008. Multiple roles of nicotine on cell proliferation and inhibition of apoptosis: implications on lung carcinogenesis. Mutat. Res. 659, 221–231.

Clancy, H.A., Sun, H., Passantino, L., Kluz, T., Munoz, A., Zavadil, J., Costa, M., 2012. Gene expression changes in human lung cells exposed to arsenic, chromium, nickel or vanadium indicate the first steps in cancer. Metallomics 4, 784–793.

Costa, A.N., Moreno, V., Prieto, M.J., Urbano, A.M., Alpoim, M.C., 2010. Induction of morphological changes in BEAS-2B human bronchial epithelial cells following chronic sub-cytotoxic and mildly cytotoxic hexavalent chromium exposures. Mol. Carcinog. 49, 582–591.

Dai, M., Wang, P., Boyd, A.D., Kostov, G., Athey, B., Jones, E.G., Bunney, W.E., Myers, R.M., Speed, T.P., Akil, H., Watson, S.J., Meng, F., 2005. Evolving gene/transcript definitions significantly alter the interpretation of GeneChip data. Nucleic Acids Res. 33, e175.

Dasari, V., Gallup, M., Lemjabbar, H., Maltseva, I., McNamara, N., 2006. Epithelial-mesenchymal transition in lung cancer: is tobacco the "smoking gun"? Am. J. Respir. Cell Mol. Biol. 35, 3–9.

Ding, X.M., 2014. MicroRNAs: regulators of cancer metastasis and epithelial-mesenchymal transition (EMT). Chin. J. Cancer 33, 140–147.

Durham, A.L., Adcock, I.M., 2015. The relationship between COPD and lung cancer. Lung Cancer 90, 121–127.

Elledge, S.J., 1996. Cell cycle checkpoints: preventing an identity crisis. Science 274, 1664–1672.

FDA, 2012. Harmful and Potentially Harmful Constituents in Tobacco Products and Tobacco Smoke. (Established List).

Federico, A., Morgillo, F., Tuccillo, C., Ciardiello, F., Loguercio, C., 2007. Chronic inflammation and oxidative stress in human carcinogenesis. Int. J. Cancer 121, 2381–2386.

Ganapathy, V., Ramachandran, I., Rubenstein, D.A., Queimado, L., 2015. Detection of in vivo DNA damage induced by very low doses of mainstream and sidestream smoke extracts using a novel assay. Am. J. Prev. Med. 48, S102–S110.

Gautier, L., Cope, L., Bolstad, B.M., Irizarry, R.A., 2004. affy—analysis of Affymetrix GeneChip data at the probe level. Bioinformatics 20, 307–315.

Gibbons, D.L., Byers, L.A., Kurie, J.M., 2014. Smoking, p53 mutation, and lung cancer. Mol. Cancer Res. 12, 3–13.

Griffiths-Jones, S., Grocock, R.J., Van Dongen, S., Bateman, A., Enright, A.J., 2006. miRBase: microRNA sequences, targets and gene nomenclature. Nucleic Acids Res. 34, D140–D144.

Grigoryeva, E.S., Kokova, D.A., Gratchev, A.N., Cherdyntsev, E.S., Buldakov, M.A., Kzhyshkowska, J.G., Cherdyntseva, N.V., 2015. Smoking-related DNA adducts as potential diagnostic markers of lung cancer: new perspectives. Exp. Oncol. 37, 5–12.

Guo, F., Parker Kerrigan, B.C., Yang, D., Hu, L., Shmulevich, I., Sood, A.K., Xue, F., Zhang, W., 2014. Post-transcriptional regulatory network of epithelial-to-mesenchymal and mesenchymal-to-epithelial transitions. J. Hematol. Oncol. 7, 19.

Health Canada, 1999. Health Canada Test Method T-115, Determination of "Tar" and Nicotine in Sidestream Tobacco Smoke.

Hecht, S.S., Stepanov, I., Carmella, S.G., 2016. Exposure and metabolic activation biomarkers of carcinogenic tobacco-specific nitrosamines. Acc. Chem. Res. 49, 106–114.

Hoffmann, R.F., Zarrintan, S., Brandenburg, S.M., Kol, A., de Bruin, H.G., Jafari, S., Dijk, F., Kalicharan, D., Kelders, M., Gosker, H.R., Ten Hacken, N.H., van der Want, J.J., van Oosterhout, A.J., Heijink, I.H., 2013. Prolonged cigarette smoke exposure alters mitochondrial structure and function in airway epithelial cells. Respir. Res. 14, 97.

Huber, W., Carey, V.J., Gentleman, R., Anders, S., Carlson, M., Carvalho, B.S., Bravo, H.C., Davis, S., Gatto, L., Girke, T., 2015. Orchestrating high-throughput genomic analysis with Bioconductor. Nat. Methods 12, 115–121.

Irizarry, R.A., Bolstad, B.M., Collin, F., Cope, L.M., Hobbs, B., Speed, T.P., 2003. Summaries of Affymetrix GeneChip probe level data. Nucleic Acids Res. 31, e15.

Iskandar, A.R., Mathis, C., Schlage, W.K., Frentzel, S., Leroy, P., Xiang, Y., Sewer, A., Majeed, S., Ortega-Torres, L., Johne, S., Guedj, E., Trivedi, K., Kratzer, G., Merg, C., Elamin, A., Martin, F., Ivanov, N.V., Peitsch, M.C., Hoeng, J., 2017. A systems toxicology approach for comparative assessment: biological impact of an aerosol from a candidate modified-risk tobacco product and cigarette smoke on human organotypic bronchial epithelial cultures. Toxicol. in Vitro 39, 29–51.

Jing, Y., Liu, L.Z., Jiang, Y., Zhu, Y., Guo, N.L., Barnett, J., Rojanasakul, Y., Agani, F., Jiang, B.H., 2012. Cadmium increases HIF-1 and VEGF expression through ROS, ERK, and AKT signaling pathways and induces malignant transformation of human bronchial epithelial cells. Toxicol. Sci. 125, 10–19.

Kalluri, R., Weinberg, R.A., 2009. The basics of epithelial-mesenchymal transition. J. Clin. Invest. 119, 1420–1428.

Kauffmann, A., Gentleman, R., Huber, W., 2009. arrayQualityMetrics—a bioconductor package for quality assessment of microarray data. Bioinformatics 25, 415–416.

Kogel, U., Gonzalez Suarez, I., Xiang, Y., Dossin, E., Guy, P.A., Mathis, C., Marescotti, D., Goedertier, D., Martin, F., Peitsch, M.C., Hoeng, J., 2015. Biological impact of cigarette smoke compared to an aerosol produced from a prototypic modified risk tobacco product on normal human bronchial epithelial cells. Toxicol. in Vitro 29, 2102–2115.

Kozomara, A., Griffiths-Jones, S., 2014. miRBase: annotating high confidence microRNAs using deep sequencing data. Nucleic Acids Res. 42, D68–73.

Li, Y., Yu, G., Yuan, S., Tan, C., Xie, J., Ding, Y., Lian, P., Fu, L., Hou, Q., Xu, B., Wang, H., 2016. 14,15-Epoxyeicosatrienoic acid suppresses cigarette smoke condensate-induced inflammation in lung epithelial cells by inhibiting autophagy. Am. J. Phys. Lung Cell. Mol. Phys. 311, L970–L980.

Mah, L.J., El-Osta, A., Karagiannis, T.C., 2010. gammaH2AX: a sensitive molecular marker of DNA damage and repair. Leukemia 24, 679–686.

Martin, F., Thomson, T.M., Sewer, A., Drubin, D.A., Mathis, C., Weisensee, D., Pratt, D., Hoeng, J., Peitsch, M.C., 2012. Assessment of network perturbation amplitudes by applying high-throughput data to causal biological networks. BMC Syst. Biol. 6, 54.

Martin, F., Sewer, A., Talikka, M., Xiang, Y., Hoeng, J., Peitsch, M.C., 2014. Quantification of biological network perturbations for mechanistic insight and diagnostics using two-layer causal models. BMC Bioinf. 15, 238.

McCall, M.N., Bolstad, B.M., Irizarry, R.A., 2010. Frozen robust multiarray analysis (fRMA). Biostatistics 11, 242–253.

Mijosek, V., Lasitschka, F., Warth, A., Zabeck, H., Dalpke, A.H., Weitnauer, M., 2016. Endoplasmic reticulum stress is a danger signal promoting innate inflammatory responses in bronchial epithelial cells. J. Innate Immun. 8, 464–478.

Momi, N., Kaur, S., Rachagani, S., Ganti, A.K., Batra, S.K., 2014. Smoking and microRNA dysregulation: a cancerous combination. Trends Mol. Med. 20, 36–47.

Morata-Tarifa, C., Jimenez, G., Garcia, M.A., Entrena, J.M., Grinan-Lison, C., Aguilera, M., Picon-Ruiz, M., Marchal, J.A., 2016. Low adherent cancer cell subpopulations are enriched in tumorigenic and metastatic epithelial-to-mesenchymal transition-induced cancer stem-like cells. Sci. Rep. 6, 18772.

Moreno-Bueno, G., Portillo, F., Cano, A., 2008. Transcriptional regulation of cell polarity in EMT and cancer. Oncogene 27, 6958–6969.

Oh, J.Y., Sin, D.D., 2012. Lung inflammation in COPD: why does it matter? F1000 Med Rep 4, 23.

Olale, F., Gerzanich, V., Kuryatov, A., Wang, F., Lindstrom, J., 1997. Chronic nicotine exposure differentially affects the function of human alpha3, alpha4, and alpha7 neuronal nicotinic receptor subtypes. J. Pharmacol. Exp. Ther. 283, 675–683.

Parekh, K., Ramachandran, S., Cooper, J., Bigner, D., Patterson, A., Mohanakumar, T., 2005. Tenascin-C, over expressed in lung cancer down regulates effector functions of tumor infiltrating lymphocytes. Lung Cancer 47, 17–29.

Reddel, R.R., De Silva, R., Duncan, E.L., Rogan, E.M., Whitaker, N.J., Zahra, D.G., Ke, Y., McMenamin, M.G., Gerwin, B.I., Harris, C.C., 1995. SV40-induced immortalization and ras-transformation of human bronchial epithelial cells. Int. J. Cancer 61, 199–205.

Reuter, S., Gupta, S.C., Chaturvedi, M.M., Aggarwal, B.B., 2010. Oxidative stress, inflammation, and cancer: how are they linked? Free Radic. Biol. Med. 49, 1603–1616.

Rodgman, A., Perfetti, T., 2013. The Chemical Components of Tobacco and Tobacco Smoke, second ed. CRC Press, pp. 2238.

Sales, G., Calura, E., Cavalieri, D., Romualdi, C., 2012. Graphite - a bioconductor package to convert pathway topology to gene network. BMC Bioinf. 13, 20.

Schaller, J.P., Keller, D., Poget, L., Pratte, P., Kaelin, E., McHugh, D., Cudazzo, G., Smart, D., Tricker, A.R., Gautier, L., Yerly, M., Reis Pires, R., Le Bouhellec, S., Ghosh, D., Hofer, I., Garcia, E., Vanscheeuwijck, P., Maeder, S., 2016. Evaluation of the tobacco heating system 2.2. Part 2: chemical composition, genotoxicity, cytotoxicity, and

physical properties of the aerosol. Regul. Toxicol. Pharmacol. 81 (Suppl. 2), S27–S47.
Smith, A.L., Hung, J., Walker, L., Rogers, T.E., Vuitch, F., Lee, E., Gazdar, A.F., 1996. Extensive areas of aneuploidy are present in the respiratory epithelium of lung cancer patients. Br. J. Cancer 73, 203–209.
Smith, M.R., Clark, B., Luedicke, F., Schaller, J.P., Vanscheeuwijck, P., Hoeng, J., Peitsch, M.C., 2016. Evaluation of the Tobacco Heating System 2.2. Part 1: description of the system and the scientific assessment program. Regul. Toxicol. Pharmacol. 81 (Suppl. 2), S17–S26.
Smyth, G.K., 2005. Limma: Linear Models for Microarray Data, Bioinformatics and Computational Biology Solutions Using R and Bioconductor. Springer, pp. 397–420.
Son, Y.O., Wang, L., Poyil, P., Budhraja, A., Hitron, J.A., Zhang, Z., Lee, J.C., Shi, X., 2012. Cadmium induces carcinogenesis in BEAS-2B cells through ROS-dependent activation of PI3K/AKT/GSK-3beta/beta-catenin signaling. Toxicol. Appl. Pharmacol. 264, 153–160.
Sun, H., Clancy, H.A., Kluz, T., Zavadil, J., Costa, M., 2011. Comparison of gene expression profiles in chromate transformed BEAS-2B cells. PLoS One 6, e17982.
Talikka, M., Kostadinova, R., Xiang, Y., Mathis, C., Sewer, A., Majeed, S., Kuehn, D., Frentzel, S., Merg, C., Geertz, M., Martin, F., Ivanov, N.V., Peitsch, M.C., Hoeng, J., 2014. The response of human nasal and bronchial organotypic tissue cultures to repeated whole cigarette smoke exposure. Int. J. Toxicol. 33, 506–517.
Team, R.C, 2014. R: A Language and Environment for Statistical Computing. 2013 R Foundation for Statistical Computing, Vienna, Austria (3-900051-07-0).
Thomson, T.M., Sewer, A., Martin, F., Belcastro, V., Frushour, B.P., Gebel, S., Park, J., Schlage, W.K., Talikka, M., Vasilyev, D.M., Westra, J.W., Hoeng, J., Peitsch, M.C., 2013. Quantitative assessment of biological impact using transcriptomic data and mechanistic network models. Toxicol. Appl. Pharmacol. 272, 863–878.
Valavanidis, A., Vlachogianni, T., Fiotakis, K., 2009. Tobacco smoke: involvement of reactive oxygen species and stable free radicals in mechanisms of oxidative damage, carcinogenesis and synergistic effects with other respirable particles. Int. J. Environ. Res. Public Health 6, 445–462.
Varemo, L., Nielsen, J., Nookaew, I., 2013. Enriching the gene set analysis of genome-wide data by incorporating directionality of gene expression and combining statistical hypotheses and methods. Nucleic Acids Res. 41, 4378–4391.
Xiao, D., He, J., 2010. Epithelial mesenchymal transition and lung cancer. J. Thorac Dis. 2, 154–159.
Zeilinger, S., Kuhnel, B., Klopp, N., Baurecht, H., Kleinschmidt, A., Gieger, C., Weidinger, S., Lattka, E., Adamski, J., Peters, A., Strauch, K., Waldenberger, M., Illig, T., 2013. Tobacco smoking leads to extensive genome-wide changes in DNA methylation. PLoS One 8, e63812.
Zhang, J., Liu, D., Feng, Z., Mao, J., Zhang, C., Lu, Y., Li, J., Zhang, Q., Li, Q., Li, L., 2016. MicroRNA-138 modulates metastasis and EMT in breast cancer cells by targeting vimentin. Biomed Pharmacother 77, 135–141.
Zhao, M., Kong, L., Liu, Y., Qu, H., 2015. dbEMT: an epithelial-mesenchymal transition associated gene resource. Sci. Rep. 5, 11459.